DRAFT

Proceedings of ICES2005
ASME Internal Combustion Engine Division 2005 Spring Technical Conference
April 5-7, 2005, Chicago, IL, USA

ICES2005-1016

EFFECT OF MULTIPLE INJECTIONS ON FUEL-AIR MIXING AND SOOT FORMATION IN DIESEL COMBUSTION USING DIRECT FLAME VISUALIZATION AND CFD TECHNIQUES

Christos A. Chryssakis
University of Michigan
2032 W.E. Lay Automotive Lab.
1231 Beal Ave.
Ann Arbor, MI 48109, USA
Phone: (734) 647-1409, fax: (734) 764-4256
cchryssa@umich.edu

Dennis N. Assanis
University of Michigan
2236 G.G. Brown Lab.
2350 Hayward Street
Ann Arbor, MI 48109, USA
Phone: (734) 764-8464
assanis@umich.edu

Sanghoon Kook
Sandia National Labs.,
Engine Combustion Department,
MS 9053, PO Box 969,
7011 East Ave.
Livermore, CA 94550, USA
Phone: (925) 294-3554
skook@sandia.gov

Choongsik Bae
Korea Advanced Institute of Science & Technology
(KAIST)
373-1 Kusong-dong
Yusong-gu
Daejeon #305-701, South Korea
Phone: +82 (42) 869-3044, fax: +82 (42) 869-5044
csbae@kaist.ac.kr

ABSTRACT

High-pressure diesel injection systems are one of the critical technologies for emission control with the assistance of electronically controlled fuel injection. Common rail injection systems have great flexibility in injection timing, pressure and multi-injections. Many studies and applications have reported the advantages of using these systems to meet the strict emissions regulations and to improve engine performance.

The main objective of this study is to investigate the effect of pilot-, post- and multiple-fuel injection strategies on fuel-air mixing and emissions formation in diesel combustion, using a combination of experimental measurements and Computational Fluid Dynamics (CFD) analysis. The experimental study was carried out on a single-cylinder optical direct-injection diesel engine equipped with a high pressure common rail fuel injection system. The experimental work was supported by CFD simulations on the single-cylinder engine in order to investigate the effect of multiple injections on mixture formation. The limitations of the soot formation model were identified through direct comparisons with experimental flame visualization.

INTRODUCTION

Direct injection diesel engines have advantages of high thermal efficiency and low fuel consumption and are penetrating in the passenger vehicle market in a fast pace. The high flexibility of common rail injection systems enables emissions reduction without sacrificing fuel economy. High injection pressures can be used in order to reduce Particulate Matter (PM) by improving spray atomization, evaporation and fuel-air mixing; however, that leads to higher cylinder temperatures that favor NO_X formation. Reducing both pollutants simultaneously can be achieved by following a multiple injection strategy, optimized for each operating condition of the engine.

Results from several contemporary investigations [1-3] show that pilot injections have the potential to reduce both NO_X and PM emissions due to improved fuel-air mixing and the reduction of the amount of diffusion combustion. Whether both pollutants or only one of them will be reduced depends on the operating conditions, the number of injections and the injection timing. Furthermore, post injections can accelerate the soot oxidation process if the injection timing and the amount of fuel are suitably selected [4]. The optimization of the injection strategy for each operating point is a complex problem with many

degrees of freedom that can be solved by extensive experimentation. CFD simulations can be used as a tool to perform parametric studies and offer insight in the fuel injection, mixing, combustion and emissions formation processes. This can be achieved by developing and implementing robust and reliable models for these processes into the CFD codes. Understanding the physical mechanisms governing the in-cylinder processes is a key step towards developing reliable models.

In order to understand the physical mechanisms leading to soot formation and oxidation a number of studies have been performed using flame visualization experiments. The development of advanced laser-based diagnostics has provided a means for making detailed measurements of the processes occurring inside of a fuel jet [5]. Over the last years laser diagnostics have been applied to direct injection diesel combustion in a variety of optically accessible engines [6-8]. These investigations have provided valuable information on diesel combustion and soot formation that can be used to evaluate and further develop computational models for use in CFD codes.

In the current work, an optically-accessible single cylinder diesel engine equipped with a common-rail injection system was built to investigate the effect of multiple injections on the combustion characteristics. The observation of the performance and emissions including the flame images could provide the explanation on the general mechanism of pollutant formations at various conditions. Optical access was possible with the elongated piston and bottom-view quartz. A high speed digital video camera was used to visualize the combustion process inside the cylinder. Experiments were carried out under a wide range of injection parameters including injection pressures and timings. The effects of multiple injections on ignition, combustion and emissions are analyzed, assisted by CFD simulations. The injection strategies selected are based on findings from previous work on the same engine [4]. Moreover, the comparison between experimental measurements and CFD results is being used to evaluate the capabilities and limitations of the current soot formation model.

EXPERIMENTAL SETUP

Optical Research Engine

The engine used in the tests is a single-cylinder, direct injection, 4-stroke optical research diesel engine equipped with a common rail injection system. The specifications of the research engine are listed in Table 1. A schematic of the engine structure is shown in Figure 1. The piston has been modified in order to permit an optical access to the combustion chamber. A quartz inserted in the piston crown (used as bowl bottom) permits a full bowl view of the combustion chamber. To collect spray and combustion images, the elongated piston accommodates an elliptical mirror reflecting the images in 45°.

For the experiments presented here, the injector is equipped with a 5-hole tip. The nominal hole diameter is 0.168 mm and the nominal angle of the fuel-jet axis was 15° downward from horizontal. Table 2 summarizes the specifications of the fuel injector.

Table 1 Engine specifications

Specifications	Resources
Bore (mm)	83
Stroke (mm)	92
Displacement (cc)	498
Compression Ratio	18.9
Stroke/Bore ratio	1.108
Swirl ratio	2.1
Con. rod length (mm)	145.8

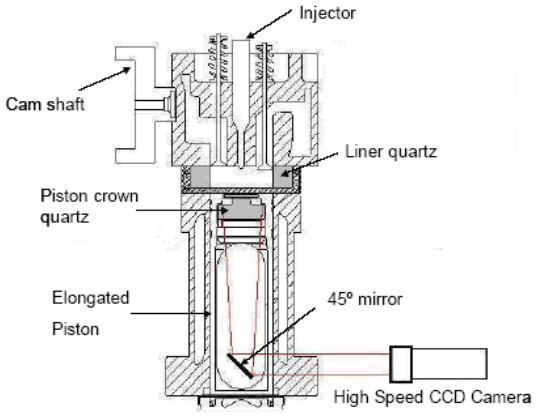

Figure 1: Schematic of the single-cylinder optical engine

Table 2 Injector Specifications

Specifications	Resources
Type	Common Rail Injection System
Injection Pressure [MPa]	0~150
Number of Holes	5
Hole Diameter [mm]	0.168
Injection Angle [deg.]	150

Engine Instrumentation

A schematic diagram of the engine test bench is shown in Figure 2. It includes the following modules: diesel engine, fuel injection equipment, data acquisition and control units as well as the emission measurement system. The electrical motor allows operation both in motoring and firing conditions. The pressure regulator valve and the solenoid injector are driven by an electronic injector operating system (TDA 3000H, TEMS Ltd.).

A shaft encoder is used to transmit the crank shaft position to the injection system and data acquisition system for the electronic control. The encoder provides two digital outputs; one is top dead center (TDC) index signal once in a revolution, and the other is the pulse train with the resolution of 0.2° crank angle (CA).

A sampling probe is installed in the exhaust pipe, which is connected to the HORIBA MEXA1500D exhaust gas analyzer. The analysis of the gaseous emissions was performed using the following instruments: non-dispersive infrared absorption (NDIR) analyzer for the CO and carbon dioxide (CO_2) measurements, chemiluminescence detector (CLD) analyzer for the NO_X measurements, flame ionization detector (FID) analyzer for the total hydrocarbon (THC) measurements. The in-line type opacimeter (OP100 EplusT Ltd.) was employed to meas-

ure the smoke emissions. If the opacimeter was used for the DI-diesel engine, the opacity of the exhaust gas represented the smoke intensity. The opacity value could be translated to Bosch smoke number by SAE J1667. The principle of opacimeter was such as an absorption photometry; while a light emitting diode emits 563 nm light and a crystal diode received it, the opacity of the exhaust gas changed the light intensity which was translated to a voltage signal.

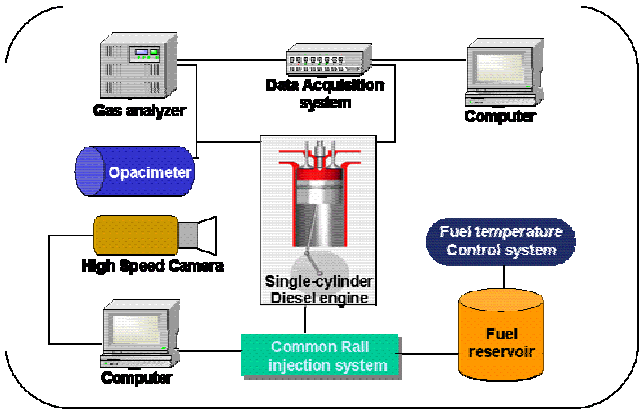

Figure 2: Schematic diagram of the engine test bench

During the tests, the injection parameters were controlled by a personal computer (PC) that was directly connected to the fuel injection system, while a Kistler 6052A piezoelectric pressure transducer was used for the measurement of the in-cylinder pressure.

The cylinder pressure data were digitized and recorded at 0.16 crank-angle-degree interval and ensemble-averaged over 130 engine cycles. The apparent heat release rate was calculated from the ensemble-averaged cylinder pressure data using the typical first law and perfect gas analysis [9].

The in-cylinder images were acquired using a high speed CCD camera (Vision Research Inc.; Phantom v7.0). It affords a high speed imaging rate of up to 10,000 frames per second so that the images could be taken every 0.48 CA at 800 rpm engine speed. The exposure times of the camera were optimized to obtain clear images. The camera images were digitized by a frame grabber in a PC to a resolution of 512 by 384 pixels. Synchronization between the engine and camera was controlled by another PC and a digital delay generator with the master signal coming from the engine shaft encoder. The camera allowed the video frame acquisition to be synchronized with the engine. This synchronization system could be adjusted to obtain images at any desired crank angle within the 0.48 degrees resolution.

Operating Conditions

All the data presented in this article were taken at an engine speed of 800rpm. Before conducting the experiments, the engine was heated to 80°C by electrical heaters in the cooling water and the lubricating oil circulation systems. The amount of pilot- and/or post-injected fuel injected was fixed at 1.5mm3/stroke. The total quantity of the fuel injected was maintained at 11.5mm3/stroke.

COMPUTATIONAL MODELS

For the numerical simulations performed in this work a modified version of the Los Alamos multi-dimensional code KIVA-3V [10-12] is been used. The modifications include the fuel injection, wall impingement, ignition, combustion and soot formation models, as described in the following paragraphs.

Computational Mesh

One inherent difficulty with modeling optical engines is the fact that the gap between the piston and the cylinder liner is considerably large. In the current experimental setup the bore diameter is equal to 83 mm and the piston diameter 81.3 mm, resulting in a gap of 0.85 mm between the piston and the cylinder wall. The effect of this geometrical feature is that there is a very strong blow-by and heat loss to the cylinder wall. The simplest way to take this effect into account is to decrease the compression ratio by increasing the squish height, so that the cylinder pressure during motoring engine operation matches the experimental measurements. In the current configuration the squish had to be increased from 1.5 mm to 3.12 mm. In Figure 3 the calculated cylinder pressure for 1.5 mm and 3.12 mm squish height is shown, as well as the experimentally measured pressure trace in the optical engine. The peak pressure of 45 bar is in reasonable agreement with the peak pressure of the multi-cylinder commercial engine that has been used as a model for the optical engine.

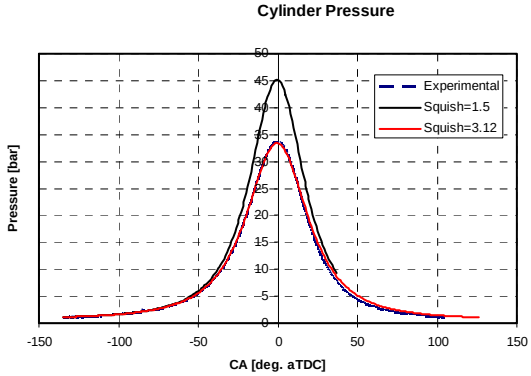

Figure 3: Cylinder Pressure Traces

In Figure 4 the computational grid is shown. Since a 5-hole nozzle is used, only a 72° sector has been modeled. The current grid contains 26,000 cells and two additional grids, one with 55,000 and one with 77,000 cells have been created in order to perform a sensitivity analysis of the grid resolution on combustion and emissions formation.

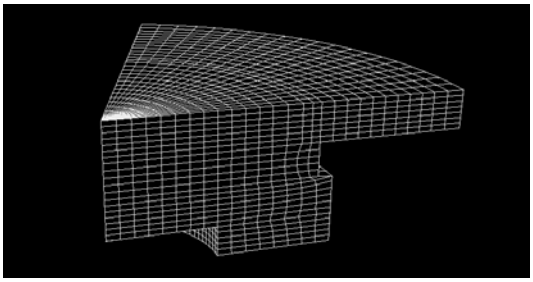

Figure 4: The computational mesh with 26,000 cells

Grid Sensitivity Analysis

Three computational grids with varying resolution have been created to model the optical engine, using 26,000, 55,000 and 77,000 cells respectively. A grid sensitivity analysis is performed to find the optimum grid resolution for the following calculations. The test case selected includes a single injection event, with Start of Injection (SOI) at 11.9° BTDC and Injection Pressure 30 MPa. Average cylinder pressure, temperature, NO_X and soot formation rate predictions were compared between the 3 grid resolutions. In Figure 5, the cylinder pressure comparison is shown and the predictions are almost identical for all three cases. Similar results are obtained for the average cylinder temperature. Therefore, the coarse grid containing 26,000 cells will be used in this work for analysis of mixture and emissions formation.

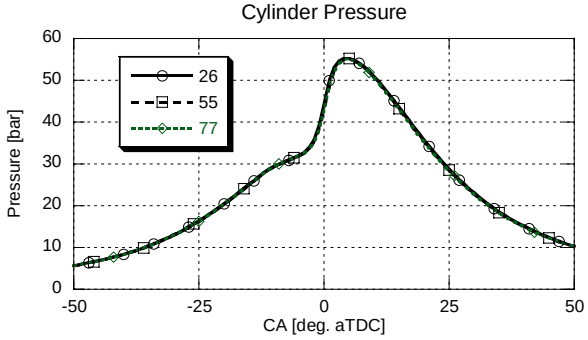

Figure 5: Grid sensitivity analysis: cylinder pressure comparison

Fuel Injection and Wall Impingement Models

The fuel spray has been modeled by assuming a liquid core emerging from the nozzle, which disintegrates very fast into droplets, with diameter equal to the nozzle diameter. The WAVE breakup model [13-16] has been adopted in this study for the secondary atomization modeling of the resulting droplets. This model is based on a linearized analysis of a Kelvin-Helmholtz instability of a stationary, round liquid jet immersed into a quiescent, incompressible gas. The result is a general dispersion equation, which relates the growth rate of an initial surface perturbation to its wavelength. Under the assumption that the size of the stripped off product droplets are proportional to the length of the fastest growing surface wave and that the rate of droplet generation is proportional to the maximal jet disturbance growth rate one obtains the expression for the radius and the time constant of the stripped off product droplet.

A wall impingement model, developed by Grover et al. [17-18] has been used to improve the prediction capability of spray-wall interactions. The model conserves mass, tangential momentum and energy of an impinging parcel. This model focuses on spray impact on dry and wet surfaces below the fuel's Leidenfrost temperature, a scenario encountered under typical engine operating conditions [19]. Three splashing parcels and one wall film parcel are used to represent the shattering of a splashing droplet upon impact with the surface. It is assumed that the impulsive force on an impinging droplet normal to the surface is dominant, thus allowing one to treat the magnitude of its tangential momentum component constant after impact. The viscous dissipation of an impinging droplet and kinetic energy of the wall film are accounted for in the energy conservation equation.

Ignition and Combustion Models

The Shell Ignition model [20] is based on a general eight-step chain-branching reaction scheme, which uses lumped kinetic parameters and other terms as coefficients in the conservation equations. The species involved are RH, the hydrocarbon fuel of the form C_nH_{2m}, O_2, R^* radical formed from the fuel, B branching agent, Q intermediate species and P products consisting of CO, CO_2 and H_2O in specific proportions. The five conservation equations that describe the above mechanism consist of a series of coupled differential equations describing the concentrations of the chemical species that influence heat release in the auto ignition process and the system temperatures.

The model used in this work is an enhanced version of the original Shell Ignition model [21]. Three main deficiencies have been recognized and eliminated in this improved version. The first one concerns the calculation of the heat release, which was based on an assumed fixed ratio CO/CO_2 in the products. This assumption has been removed and the heat release is given instead by an energy balance. The second modification is related to the inert products of the two termination reactions. In the previous scheme, radicals are removed from the reactants pool by converting them into N_2. Here, it is assumed that the two radical termination reactions lead to the same species that would result from the combustion of the same initial mixture of reactants. The third modification is related to the Shell species R^*, B and Q. In the previous scheme the contribution of these species to the energy balance was ignored. In the present scheme enthalpy values for these generic species have been assigned.

The Characteristic-Time Combustion (CTC) model [22], is used for combustion simulations. The rate of change of the mass fraction of species m, Y_m, due to chemical reaction is given by:

$$\frac{dY_m}{dt} = -\frac{Y_m - Y_m^*}{\tau_c} \tag{6}$$

where τ_c is the characteristic time of combustion and Y_m^* denotes the local equilibrium mass fraction. The characteristic time is assumed to be the same for all seven species (fuel, O_2, N_2, CO, CO_2, H_2, H_2O) considered necessary to predict the thermodynamic equilibrium temperatures. Also, the characteristic time is the weighted sum of a laminar time scale, τ_l, and a turbulent time scale, τ_t, given by:

$$\tau_c = \tau_l + f\,\tau_t, \tag{7}$$

where the weight function f simulates the influence of turbulence on combustion after ignition has taken place. The turbulent time scale is proportional to the eddy turnover time

$$\tau_t = C_M k/\varepsilon. \tag{8}$$

The constant C_M is an input variable that acts as a scaling parameter between the different engines and their injection configurations

Soot and NO_X Formation Models

The Extended Zeldovich Mechanism, as given by Heywood [9] has been used to predict NO formation from diesel combustion. The principal reactions for NO formation and destruction are:

$$O + N_2 \leftrightarrow NO + N$$
$$N + O_2 \leftrightarrow NO + O$$
$$N + OH \leftrightarrow NO + H$$

The soot formation model developed by Hiroyasu and modified by Han et al. [18] has been used throughout this work. The model predicts the production of soot mass, M_s, by a single-step competition between the soot mass formation rate, $\dot{M}_{sf}$, and the soot mass oxidation rate, $\dot{M}_{so}$, according to:

$$\frac{dM_s}{dt} = \dot{M}_{sf} - \dot{M}_{so}. \quad (9)$$

The Arrhenius formation rate is proportional to the fuel vapor mass, M_{fv}, and the formation coefficient is a function of pressure and temperature, according to:

$$K_f = A_{sf} P^{1/2} \exp(-E_{sf}/RT). \quad (10)$$

The Arrhenius oxidation rate is proportional to the soot mass and the oxidation coefficient is a function of pressure, temperature and the oxygen mole fraction. The original model has been modified by replacing the Arrhenius global oxidation rate equation with the experimentally based oxidation rate of Nagle and Strickland-Constable (NSC) [22].

This simplified two-step empirical model for soot formation offers the advantage of easy implementation and adjustment but caution must be paid when considering the predicted spatial distribution, as shown by Tao et al. [23]. Similar conclusions have been reached through this work and some of the limitations of the model are revealed through comparison with optical diagnostics measurements.

FUEL-AIR MIXING AND SOOT FORMATION

The effect of multiple injection strategies on fuel-air mixing and emissions formation has been studied by investigating both single and split injection schemes, including two and three injection events per cycle, namely pilot-main, main-post and pilot-main-post [4]. In the current work, a number of these cases are used for comparison with CFD calculations in order to explore the capabilities and limitations of the soot formation model. The ignition and combustion characteristics for each case are checked by comparing experimentally measured cylinder pressure traces with CFD results.

Single Injections

Two single injection cases, with SOI -15° aTDC and -5° aTDC are considered here to show the effects of injection timing on soot formation. In Figure 6 the experimentally measured cylinder pressure traces for both cases are shown, as well as the predictions with KIVA-3V. The predicted pressure agrees well with the experimental measurements in both cases, implying that the combustion process is successfully modeled. The small discrepancies observed in Figure 6 are attributed to the fact that the compression ratio had to be lowered in order to take into account the significant blow-by losses that could not be modeled otherwise with KIVA. In most cases simulated similar small differences are observed; however, the ignition and combustion models can successfully be used to predict a wide range of conditions, including split injections, without changing the calibration.

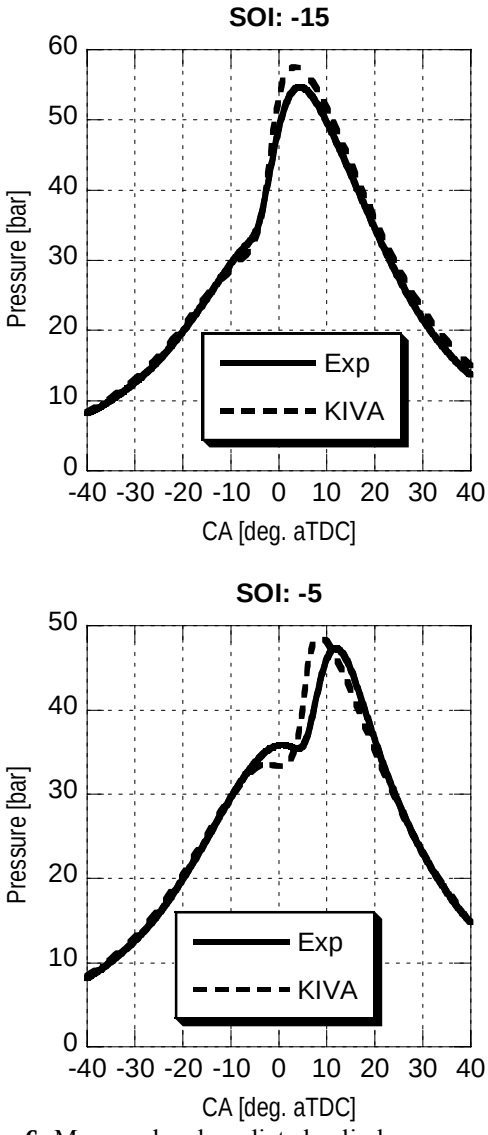

Figure 6: Measured and predicted cylinder pressure

In Figure 7 soot luminosity images are shown for SOI=-15° aTDC. The first visible flame is apparent at -7° aTDC at

the center of the cylinder, near the injector nozzle tip, and propagates toward the cylinder walls. The timing of the first visible flame roughly coincides with the ignition timing. It is interesting to note that the injection duration in this case is about 5° CA; therefore, the injection process has been completed at -10° aTDC. However, the first luminosity images, close to the injector tip, imply that soot is being formed and oxidized in this area after the end of injection.

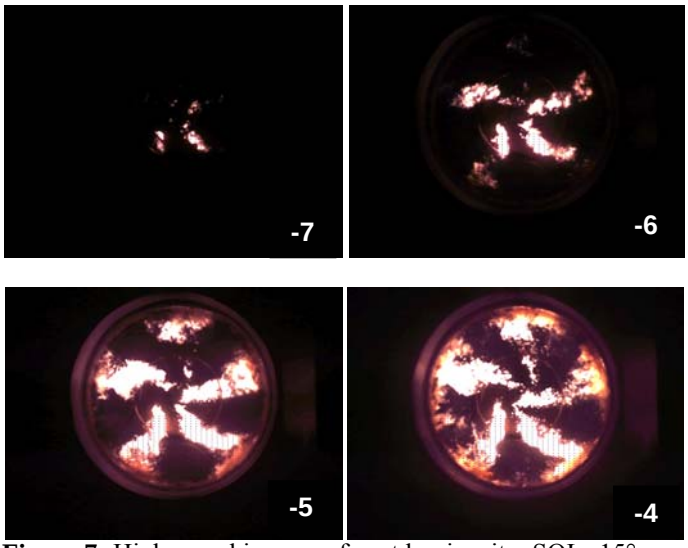

Figure 7: High-speed images of soot luminosity, SOI=-15°

In Figure 8 CFD predictions of the soot formation process are presented. The images are substantially different than the experimental ones both temporally and spatially: soot appears for the first time -4° aTDC (3° later than in the experimental images) but the most striking difference is that soot is initiated in the area close to the cylinder walls. This can be explained considering that the soot formation model uses only fuel vapor as soot precursor and therefore creates soot at locations with high vapor concentration.

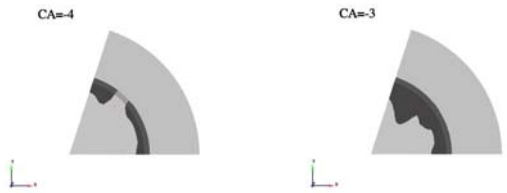

Figure 8: CFD predictions of soot formation, SOI=-15° aTDC

In order to explain these contradicting results, the fuel-air mixing history was studied. In Figure 9 the equivalence ratio is shown as a function of time during the injection process. The isosurface plotted represents equivalence ratio of 2.0 and higher.

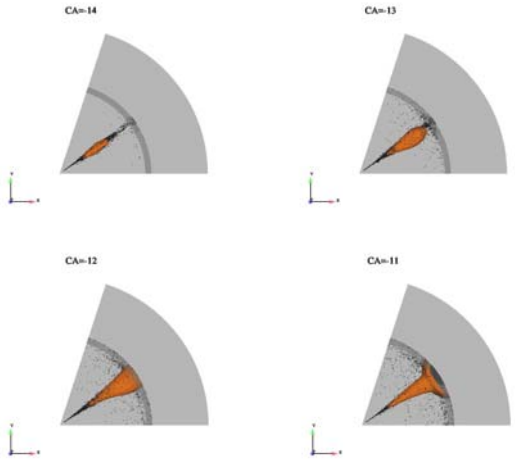

Figure 9: CFD predictions: isosurface of equivalence ratio 2.0, SOI=-15°

The structures of the isosurfaces shown in Figure 9 are very similar in shape and evolution with the soot luminosity structures acquired experimentally using the high-speed camera. However, there is a delay of approximately 7° CA, which corresponds to 1.46 msec. It seems that the CFD images show the location where the soot precursors start forming. Small particles start forming in rich areas (φ>2.0) close to the nozzle. As the fuel spray propagates into the cylinder and reaches the cylinder wall, the reach areas extend to the wall as well, initiating the formation of soot precursors. It appears that a certain amount of time is required from the onset of the soot precursors formation until the moment when soot particles grow and start oxidizing, which is the process captured in the experimental high-speed images. Observation of Figures 7 and 9 also reveals that the soot particles are found roughly in the same location where the precursors started forming. They are only slightly transported due to the swirl motion in the cylinder.

The observations made for SOI=-15° aTDC were verified with similar observations for SOI=-5° aTDC. Figures 10 and 11 show experimental high-speed images of soot luminosity and CFD predictions of equivalence ratio isosurfaces, respectively. Exactly the same time delay of 7° CA or 1.46 msec is observed in this case between the moment when the equivalence ratio of 2.0 starts forming until the first visible luminosity images in the experiment.

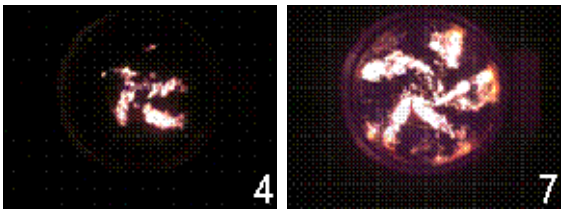

Figure 10: High-speed images of soot luminosity, SOI=-5°

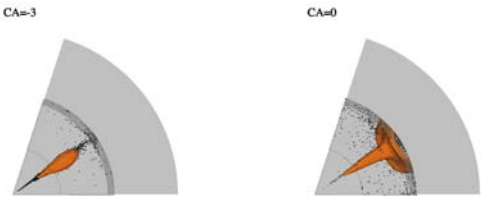

Figure 11: CFD predictions: isosurface of equivalence ratio 2.0, SOI=-5°

The simplified soot formation model fails to predict the correct location of soot initiation in this case as well. In Figure 12 the CFD predictions for soot formation are shown, indicating that soot should appear first close to the cylinder walls.

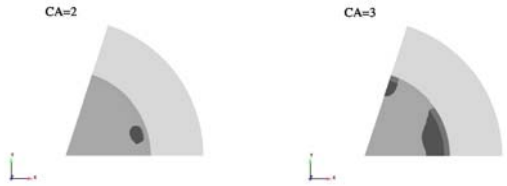

Figure 12: CFD predictions of soot formation, SOI=-5° aTDC

This set of results indicates that the simplified two-step soot formation model is not adequate for predicting correctly the location where soot first appears in the cylinder. However, it is interesting to note, that with appropriate calibration of its constant it can predict the correct amount of soot mass in the cylinder.

Pilot Injections

Further investigation of the soot formation process has been performed using a split injection strategy, employing a pilot and a main injection event. The case discussed here involves a pilot injection timing at -26° aTDC and the main injection set at -6.5° aTDC. Figure 13 shows the cylinder pressure comparison between the experiment and the CFD calculation. There is only a small disagreement close to the ignition point, indicating a slightly longer ignition delay in the CFD calculation, but overall the agreement is acceptable.

Figures 14 and 15 show the experimental images of soot luminosity and CFD images of the equivalence ratio isosurface (φ=2.0). Even though the pilot injection starts at -26° aTDC, there is no fuel-rich area observed in the cylinder following this injection event. This is attributed to relatively low cylinder temperatures that do not allow for fast fuel evaporation, as well as to the small fuel quantity injected. The first fuel-rich area is apparent shortly after the main injection event. The structures observed are very similar to the experimentally acquired soot luminosity images. In this case the time delay is slightly shorter than for the single injection case, approximately 5° CA, which corresponds to 1.04 msec. This observation is in agreement with the conclusions reached by Park et al. [16] who found that pilot injections are effective in shortening the ignition delay and that soot precursors formed by pilot injections are easily converted into soot as the main injection starts. Soot predictions from KIVA are inaccurate in this case as well, showing initiation of soot formation close to the walls, similarly to the previous cases.

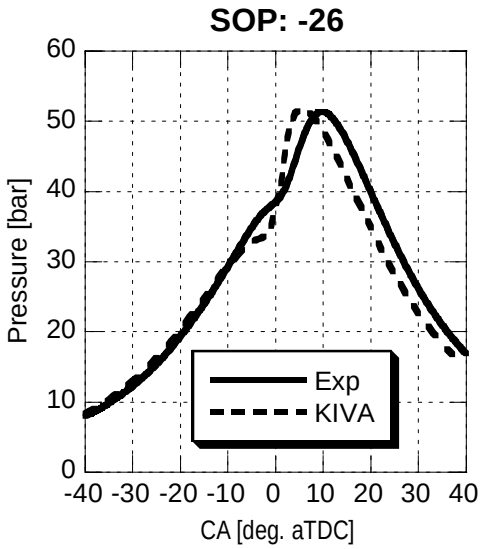

Figure 13: Measured and predicted cylinder pressure, pilot-main injections

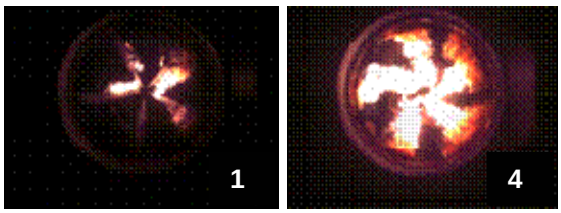

Figure 14: High-speed images of soot luminosity, pilot-main injections

The effect of pilot injections on engine performance and soot emissions is demonstrated in Figure 16. The engine IMEP increases up to 20% when a pilot injection is employed but there is a considerable penalty in soot emissions (opacity) because of the extended diffusion-controlled combustion. An additional advantage of the pilot injection is the suppression of NO_X emissions and combustion noise [16]. Moreover, it was reported in [16] that the soot emissions can be reduced by employing a post injection that enhances soot oxidation when timed appropriately. Therefore, a triple injection approach, with pilot-main-post injections, has been studied in order to combine the advantages of the two methods.

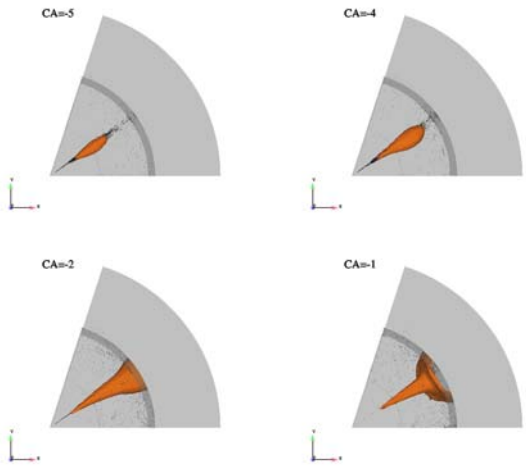

Figure 15: CFD predictions: isosurface of equivalence ratio 2.0, pilot-main injections

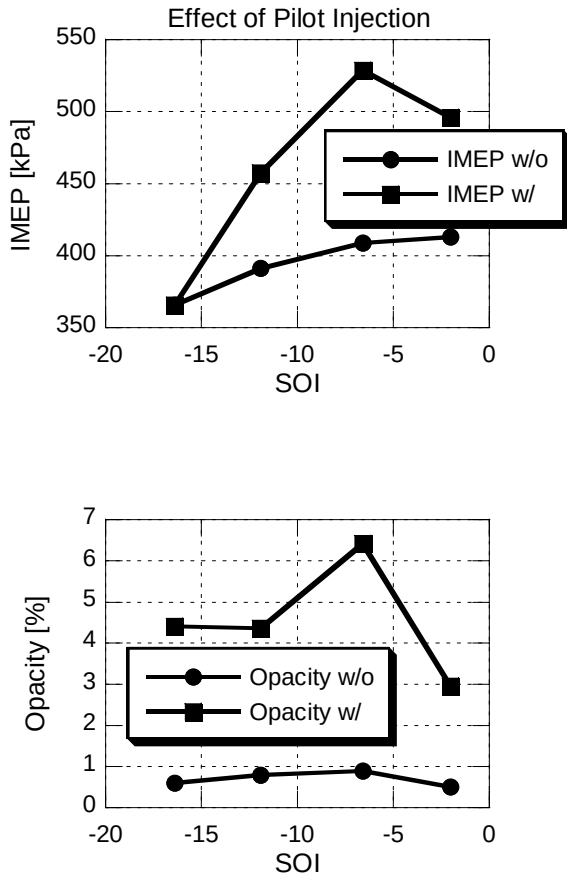

Figure 16: Effect of pilot injection on IMEP and smoke formation; Start of Pilot: 20° bSOI

Triple Injections

The final part of this investigation includes a triple injection strategy. The pilot injection was set at -35° aTDC, the main at -5° aTDC and the post at +15° aTDC. As shown in Figure 17, the soot luminosity first appears at -13° aTDC, almost 30° or 6.25 msec after the pilot injection is completed. CFD calculations of the equivalence ratio, shown in Figure 17, reveal that there is a slightly rich fuel vapor concentration in this location during the pilot injection. The isosurfaces in Figure 18 represent equivalence ratio of 1.25 instead of 2.0, as in previous images. An equivalence ratio of 2.0 could not be detected in these early timings. It is believed that this fuel vapor initiates the soot growing process, with soot precursors developing at this location, close to the nozzle. The longer time delay is attributed to colder cylinder temperatures and lower fuel concentrations, therefore soot precursors require longer time to grow into soot particles and start oxidizing. It is very interesting to note that in the experimental images the luminosity is weaker than in previous cases and does not extend along the cylinder wall. Likewise, the CFD rich vapor concentration pockets are observed only for a short period of time along the spray axis and they become leaner as they reach the wall. This is strong evidence that soot precursors first appear in these rich pockets.

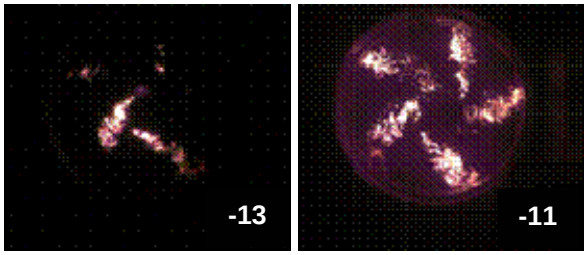

Figure 17: High-speed images of soot luminosity, triple injections

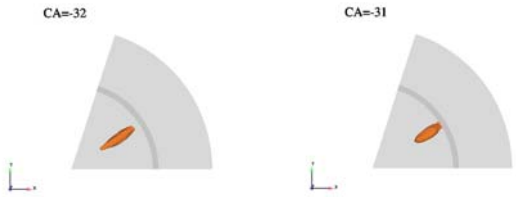

Figure 18: CFD predictions: isosurface of equivalence ratio 1.25, triple injection

Most of the soot produced in the triple injection case is formed after the main injection event. In Figure 19 it appears that soot starts forming at 2° aTDC and gradually expands to the cylinder walls. Exactly the same trend is evident from the equivalence ratio isosurfaces, shown in Figure 20. The time delay in this case is shorter, in the order of 4°-5°, which corresponds to approximately 1 msec. This shorter delay is most likely due to the already existing soot and fuel vapor in the cylinder. The same trend was observed for the pilot-main injection case.

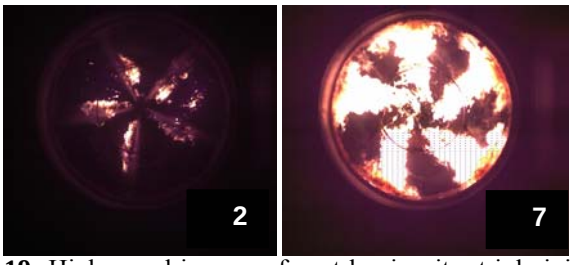

Figure 19: High-speed images of soot luminosity, triple injections

Figure 20: CFD predictions: isosurface of equivalence ratio 2.0, triple injection

In Figure 21 the soot and NO_X measurements for this triple injection strategy are shown. Both pollutants are reduced compared to the single injection case with SOI=-5° aTDC. The NO_X reduction in the triple injection case is attributed to the shorter ignition delay, caused by the pilot injection; consequently. The amount of premixed combustion is reduced. The reduction in smoke emissions has been achieved through the post-injection which enables oxidation of the soot formed during the main injection event. Furthermore, less soot is formed because of diffusion combustion during the main injection, since the amount of fuel injected has been reduced and the remaining fuel is used for the post injection. The IMEP for the triple injection case has been reduced only by 3% compared to the single injection.

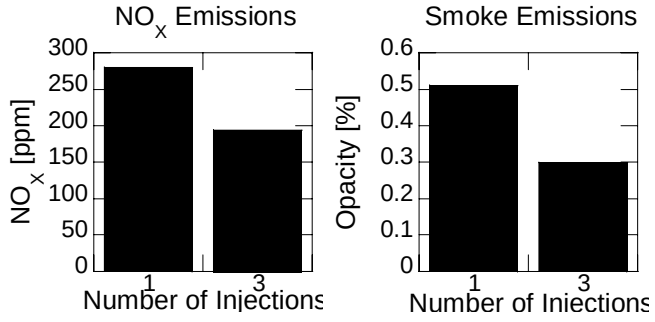

Figure 21: Effect of triple injection on soot and NO_X emissions

CONCLUSIONS

The effect of multiple injections on diesel combustion has been studied using experimental flame visualization techniques assisted by CFD simulations. It has been shown that multiple injection strategies can be successfully used to simultaneously reduce smoke and NO_X emissions. The pilot injection reduces the ignition delay and therefore the amount of premixed combustion, leading to lower temperatures and NO_X emissions, but significantly increases soot emissions by increasing the diffusion combustion. Employing a post-injection combined with a pilot injection results in reduced soot formation from diffusion combustion and enhances the soot oxidation process during the expansion stroke, resulting in decreased smoke emissions, while the NO_X concentration is maintained in low levels.

The comparison between CFD predictions and experimental measurements shows that soot precursors start forming in fuel-rich areas of the combustion chamber, typically surrounding the fuel jet. There is a time delay between the timing when the fuel-rich areas are created and the timing when the soot oxidation process is observed experimentally. This delay is interpreted as the time required for the soot particles to grow and start oxidizing. When pilot injections are employed the time delay is shortened, implying faster growth rate. Finally, it has been found that the soot formation model currently used cannot correctly predict the location of soot initiation and evolution. More sophisticated models are needed for reliable calculations of soot formation from CFD codes.

ACKNOWLEDGMENTS

The authors would like to acknowledge the support of the National Research Laboratory of Korea and the BK21 collaboration program between KAIST and The University of Michigan. Also, Nicolas Herauville, Vassilis Hamosfakidis and Kristina Reslin van Dort are acknowledged for their assistance with creating the computational grid and performing the parametric studies.

REFERENCES

1. Benajes, J., Molina, S., Garcia, J.M., "Influence of Pre- and Post-Injection on the Performance and Pollutant Emissions in a HD Diesel Engine", SAE Technical Paper Series 2001-01-0526, 2001
2. Payri, F., Benajes, J., Pastor, J.V., Molina, S., "Influence of the Post-Injection Pattern on Performance, Soot and NO_X Emissions in a HD Diesel Engine", SAE Technical Paper Series 2002-01-0502, 2002
3. Ishikawa, N., Uekusa, T., Nakada, T., Hariyoshi, R., "DI Diesel Emission Control by Optimized Fuel Injection", SAE Technical Paper Series 2004-01-0117, 2004
4. Park, C., Kook, S., Bae, C., "Effects of Multiple Injections in a HSDI Diesel Engine Equipped with Common Rail Injection System", SAE Technical Paper Series, 2004-01-0127, 2004
5. Dec., J.E., "A Conceptual Model of DI Diesel Combustion Based on Laser-Sheet Imaging", SAE Technical Paper Series 970873, 1997
6. Lee, W., Solbrig, C.E., Litzinger, T.A., Santoro, R.J., Santavicca, D.A., "Planar Laser Light Scattering for the In-Cylinder Study of Soot in a Diesel Engine", *SAE Transactions*, vol. 99, Sec. 3, pp. 2222-2235, SAE Technical Paper Series 902125, 1990
7. Dec, J.E., zur Loye, A.O., Siebers, D.L., "Soot Distribution in a D.I. Diesel Engine Using 2-D Laser-Induced Incandescence Imaging", *SAE Transactions*, vol. 100, Sec. 3, pp. 277-288, SAE Technical Paper Series 910224, 1991
8. Alatas, B., Pinson, J.A., Litzinger, T.A., Santavicca, D.A., "A Study of NO and Soot Evolution in a D.I. Diesel Engine via Planar Imaging", *SAE Transactions*, vol. 102, Sec.

3, pp. 1463-1473, SAE Technical Paper Series 930973, 1993
9. Heywood, J.B., *Internal Combustion Engine Fundamentals*, McGraw-Hill, 1988
10. A.A. Amsden, P.J., O'Rourke and T.D. Butler, "KIVA II – A Computer Program for Chemically Reactive Flows with Sprays", Los Alamos National Laboratory LA-11560-MS, 1989
11. A.A. Amsden, "KIVA-3: A KIVA Program with Block-Structured Mesh for Complex Geometries", Los Alamos National Laboratory LA-12503-MS, 1993
12. Amsden A.A., "KIVA-3V: A Block-Structured KIVA Program for Engines with Vertical or Canted Valves", Los Alamos National Laboratory LA-13313-MS, July 1997
13. Reitz, R.D., Diwakar, R., "Structure of High-Pressure Fuel Sprays", SAE Technical Paper Series 870598, 1987
14. Reitz, R.D., "Modeling Atomization Processes in High-Pressure Vaporizing Sprays", *Atomisation and Spray Technology*, 3, pp. 309-337, 1987
15. Liu, A.B., Reitz, R.D., "Mechanisms of Air-Assisted Liquid Atomization", *Atomization and Sprays*, 3, pp. 55-75, 1993
16. Liu, A.B., Mather, D., Reitz, R.D., "Modeling the Effects of Drop Drag and Breakup on Fuel Sprays", SAE Technical Paper Series 930072, 1993
17. Grover, R.O., Assanis, D.N., "A Spray Wall Impingement Model Based Upon Conservation Principles," 5th International Symposium on Diagnostics and Modeling of Combustion in Internal Combustion Engines, pp. 551-559, 2001
18. Grover, R.O., Assanis, D.N., Lippert, A.M., El Tahry, S.H., Drake, M.C., Fansler T.D., Harrington D.L., "A Critical Analysis of Splash Criteria for GDI Spray Impingement", 15th Annual Conference on Liquid Atomization and Spray Systems, Madison, WI, May 2002
19. Han, Z., Xu, Z., Trigui, N., "Spray/Wall Interaction Models for Multidimensional Engine Simulation", *International Journal of Engine Research*, **1**, pp. 127-146, 2000
20. Halstead, M.P., Kirsch, L.J., Prothero, A., Quinn, C.P., *Proc. R. Soc. Lond.,* 346, 1975
21. Hamosfakidis, V., Reitz, R.D., "Optimization of a hydrocarbon fuel ignition model for two single component surrogates of diesel fuel", *Combustion and Flame,* **132**, pp. 433-450, 2003
22. Han, Z., Uludogan, A., Hampson, G.J., Reitz, R.D., "Mechanism of Soot and NO_X Emission Reduction Using Multiple-Injection in a Diesel Engine", SAE Technical Paper Series, 960633, 1996
23. Tao, F., Srinivas S., Reitz, R.D., Foster, D.E., "Current Status of Soot Modeling Applied to Diesel Combustion Simulations", COMODIA 2004, Yokohama, Japan, August 2004